Mode-division multiplexed transmission with inline few-mode fiber amplifier

Neng Bai,[1,6] Ezra Ip,[1,*] Yue-Kai Huang,[1] Eduardo Mateo,[1] Fatih Yaman,[1] Ming-Jun Li,[2] Scott Bickham,[2] Sergey Ten,[2] Jesús Liñares,[3] Carlos Montero,[3] Vicente Moreno,[3] Xesús Prieto,[3] Vincent Tse,[4] Kit Man Chung,[4] Alan Pak Tao Lau,[4] Hwa-Yaw Tam,[4] Chao Lu,[4] Yanhua Luo,[5] Gang-Ding Peng,[5] Guifang Li,[6] and Ting Wang[1]

[1]NEC Labs America, 4 Independence Way, Princeton, NJ 08540, USA
[2]Corning Incorporated, 1 Riverfront Plaza, Corning, NY 14831, USA
[3]Faculty of Physics and School of Optics and Optometry, University of Santiago de Compostela, Santiago de Compostela, Spain
[4]Department of Electrical Engineering, The Hong Kong Polytechnic University, Hong Kong, China
[5]School of Electrical Engineering & Telecommunications, University of New South Wales, Sydney, Australia
[6]The College of Optics & Photonics, University of Central Florida, Orlando, FL 32816, USA
[*]ezra.ip@nec-labs.com

Abstract: We demonstrate mode-division multiplexed WDM transmission over 50-km of few-mode fiber using the fiber's LP_{01} and two degenerate LP_{11} modes. A few-mode EDFA is used to boost the power of the output signal before a few-mode coherent receiver. A 6×6 time-domain MIMO equalizer is used to recover the transmitted data. We also experimentally characterize the 50-km few-mode fiber and the few-mode EDFA.

OCIS codes: (060.2360) Fiber optics links and subsystems; (060.2330) Fiber optics communications.

References and links

1. D. Qian, M.-F. Huang, E. Ip, Y.-K. Huang, Y. Shao, J. Hu, and T. Wang, "101-Tb/s (370×294-Gb/s) PDM-128QAM-OFDM transmission over 3×55-km SSMF using pilot-based phase noise mitigation," in Proc. OFC (Los Angeles, CA, USA 2011). Paper PDPB5.
2. J. Sakaguchi, Y. Awaji, N. Wada, A. Kanno, T. Kawanishi, T. Hayashi, T. Taru, T. Kobayashi, and M. Watanabe, "109-Tb/s (7×97×172-Gb/s SDM/WDM/PDM) QPSK transmission through 16.8-km heterogeneous multi-core fiber," in Proc. OFC (Los Angeles, CA, USA 2011). Paper PDPB6.
3. R. Ryf, A. Sierra, R.-J. Essiambre, A. H. Gnauck, S. Randel, M. Esmaeelpour, S. Mumtaz, P. J. Winzer, R. Delbue, P. Pupalaikis, A. Sureka, T. Hayashi, T. Taru, and T. Sasaki, "Coherent 1200-km 6×6 MIMO mode-multiplexed transmission over 3-core microstructured fiber," in 37th European Conference and Exposition on Optical Communications, OSA Technical Digest (CD) (Optical Society of America, 2011), paper Th.13.C.1.
4. S. Randel, R. Ryf, A. Sierra, P. J. Winzer, A. H. Gnauck, C. A. Bolle, R. J. Essiambre, D. W. Peckham, A. McCurdy, and R. Lingle, Jr., "6×56-Gb/s mode-division multiplexed transmission over 33-km few-mode fiber enabled by 6×6 MIMO equalization," Opt. Express **19**(17), 16697–16707 (2011).
5. E. Ip, N. Bai, Y. Huang, E. Mateo, F. Yaman, S. Bickham, H. Tam, C. Lu, M. Li, S. Ten, A. P. T. Lau, V. Tse, G. Peng, C. Montero, X. Prieto, and G. Li, "88×3×112-Gb/s WDM Transmission over 50-km of Three-Mode Fiber with Inline Multimode Fiber Amplifier," in 37th European Conference and Exposition on Optical Communications, OSA Technical Digest (CD) (Optical Society of America, 2011), paper Th.13.C.2.
6. N. Bai, E. Ip, T. Wang, and G. Li, "Multimode fiber amplifier with tunable modal gain using a reconfigurable multimode pump," Opt. Express **19**(17), 16601–16611 (2011).
7. Y. Yung, S. Alam, Z. Li, A. Dhar, D. Giles, I. Giles, J. Sahu, L. Grüner-Nielsen, F. Poletti, and D. Richardson, "First demonstration of multimode amplifier for spatial division multiplexed transmission systems," in 37th European Conference and Exposition on Optical Communications, OSA Technical Digest (CD) (Optical Society of America, 2011), paper Th.13.K.4.
8. R. Ryf, A. Sierra, R. Essiambre, S. Randel, A. Gnauck, C. A. Bolle, M. Esmaeelpour, P. J. Winzer, R. Delbue, P. Pupalaikis, A. Sureka, D. Peckham, A. McCurdy, and R. Lingle, "Mode-Equalized Distributed Raman Amplification in 137-km Few-Mode Fiber," in 37th European Conference and Exposition on Optical Communications, OSA Technical Digest (CD) (Optical Society of America, 2011), paper Th.13.K.5.
9. J. Liñares, C. Montero, V. Moreno, M. C. Nistal, X. Prieto, J. R. Salgueiro, and D. Sotelo, "Glass processing by ion exchange to fabricate integrated optical planar components: applications," Proc. SPIE **3936**, 227–238 (2000).

#157732 - $15.00 USD Received 7 Nov 2011; revised 12 Dec 2011; accepted 13 Dec 2011; published 20 Jan 2012

10. J. R. Salgueiro, V. Moreno, and J. Liñares, "Model of linewidth for laser writing on a photoresist," Appl. Opt. **41**(5), 895–901 (2002).
11. E. Ip and J. M. Kahn, "Digital equalization of chromatic dispersion and polarization mode dispersion," J. Lightwave Technol. **25**(8), 2033–2043 (2007).

1. Introduction

As the capacity of optical systems based on single mode fiber (SMF) approach the nonlinear Shannon's limit [1], further capacity growth requires new transmission paradigm. Time-division multiplexing (TDM) and wavelength-division multiplexing (WDM) are examples of parallel transmission in time/frequency which have been successfully employed in SMF systems. To further increase the number of parallel channels, the spatial dimensions may be exploited. Indeed, space-division multiplexing (SDM) is gaining prominence as the most promising technology for overcoming the capacity crunch. To date, SDM transmission has been reported for three fiber types: these are weakly coupled multicore fibers (MCF) [2], strongly coupled MCF [3], and multimode fibers (MMF) [4,5]. Weakly coupled MCFs behave like parallel SMF channels, and have the lowest decoding complexity per bit. However, the achievable information capacity per unit area is low. By contrast, both strongly coupled MCF and MMF require multiple-input multiple-output (MIMO) detection techniques with high decoding complexity, but can achieve higher information capacity per unit area.

In principle, the capacity of SDM transmission scales linearly with the number of parallel channels, i.e., the number of modes per core multiplied by the number of cores in the fiber. The same capacity increase, however, can also be obtained by using parallel SMF fibers. To make SDM systems competitive with parallel SMF, it is necessary to integrate devices such as inline amplifiers, as well as simplify the digital signal processing (DSP) requirement so that power consumption is manageable. Erbium-doped fiber amplifiers based on FMF was studied in [6], and was recently demonstrated in [5] and [7]; while Raman amplification in FMF was studied in [8]. The highest capacity reported to date over FMF, which employed both WDM and mode-division multiplexing (MDM), was 88 × 3 × 112-Gb/s using only the C-band [5]. In this paper, we will furnish further details of the WDM-MDM transmission. The outline of the paper is as follows: in Section 2, we measure the characteristics of the FM-EDFA. In Section 3, the experimental setup for WDM-MDM transmission is introduced. Experimental results are presented in Section 4, including results for performance versus algorithmic complexity. In Section 5, the modal group delay and chromatic dispersion characteristics of the FMF are characterized.

2. Few-mode EDFA

A few-mode erbium-doped fiber amplifier (FM-EDFA) was constructed out of 15 meters of few-mode erbium-doped fiber. Originally intended as a step-index profile fiber with a uniformly doped core, the actual refractive index profile measured in the radial direction is shown in Fig. 1(a). The FM-EDF supports two mode groups at the signal wavelength (around 1550 nm): $LP_{01}^{(s)}$ and $LP_{11}^{(s)}$, and four mode groups at the pump wavelength (around 980 nm): $LP_{01}^{(p)}$, $LP_{11}^{(p)}$, $LP_{21}^{(p)}$ and $LP_{02}^{(p)}$. Normalized intensity distributions for the signal and pump modes of interest are shown in Fig. 1(b).

To characterize the FM-EDFA, we use the experiment setup shown in Fig. 2. A tunable C-band external cavity laser (ECL) is amplified and passed through a polarization controller (PC), and is then spatially transformed by a mode multiplexer. The mode multiplexer splits the input signal into two paths. The single-mode fiber in each path is terminated by a beam collimator (BC) with focal length of 11 mm. At one of the paths, a phase plate (PP) converts the LP_{01} Gaussian beam into an LP_{11} mode. The two beams are passively combined by a passive beam splitter (BS) and launched into two meters of undoped FMF of the same type as the 50-km FMF used in the transmission experiment described in Section 3 which supports the propagation of LP_{01} and LP_{11} modes at the signal wavelength. At the FM-EDFA, the FMF

#157732 - $15.00 USD Received 7 Nov 2011; revised 12 Dec 2011; accepted 13 Dec 2011; published 20 Jan 2012

is terminated at another 11-mm BC. A dichoric mirror (DM) spatially combines the signal beam with a 980 nm forward pump beam, which is collimated by an 8-mm BC followed by an optional PP. The spatially overlapping signal and pump are launched into the FM-EDF whose ends are spliced with short sections of undoped FMF. At the output of the FM-EDFA, another 980nm pump beam is collimated by an 8-mm BC and spatially transformed by an optional PP. After reflection by a DM, the beam is launched into the output of FM-EDF as a counter propagating pump. We angle-cleave the output facet of the FM-EDF to minimize reflections back into the amplifying medium, and terminated the fiber at an 11-mm BC. Two DMs are used to filter the unused pump, allowing the signal power and beam profile to be measured.

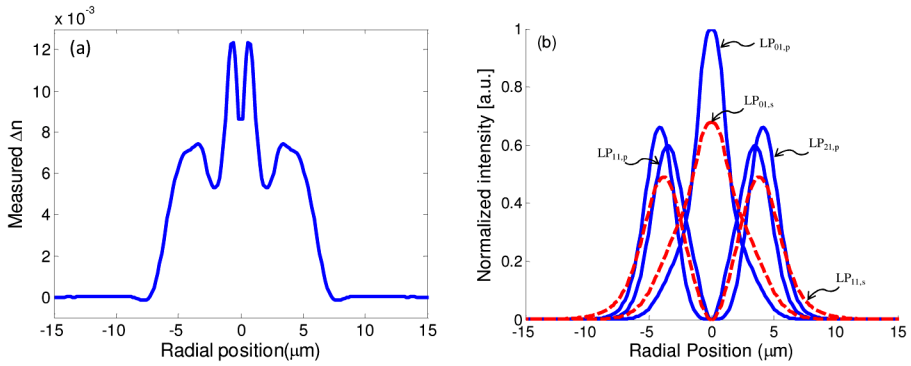

Fig. 1. (a) Refractive index of MM-EDF, (b) Normalized radial intensity profiles of signal and pump modes.

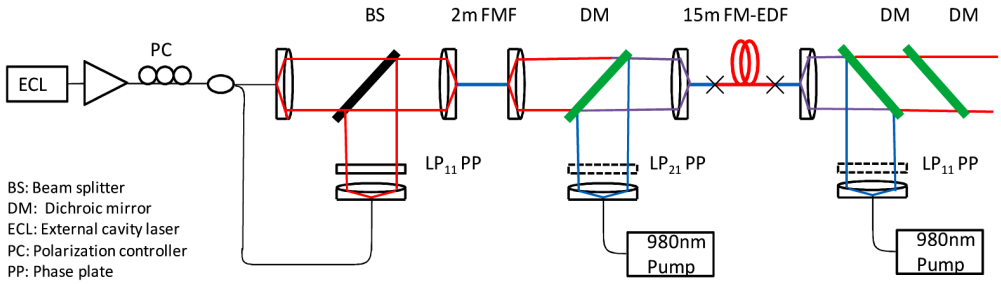

Fig. 2. Experiment setup.

We measured coupling losses of our setup to be: 1.8 dB and 3.9 dB for coupling between single-mode fiber and the LP_{01} and LP_{11} modes at the signal wavelength; and 5dB, 7.2 dB and 9.6 dB for coupling between single-mode fiber and the LP_{01}, LP_{11} and LP_{21} modes at the pump wavelength. The higher losses for the pump are due to chromatic dispersion, which causes the BC to have different focal lengths at the signal and pump wavelengths. Since the position of the terminated fiber is optimized for the signal wavelength in the BC, the pump beam is not well focused. Figures 3(a) and 3(b) show the modal gain measured for $LP_{01}^{(s)}$ and $LP_{11}^{(s)}$ when forward pumping in $LP_{01}^{(p,f)}$ and $LP_{21}^{(p,f)}$, after account for all coupling losses. As Figs. 3(c) and 3(d) show, the modal gain were also measured when backward pumping in $LP_{01}^{(p,b)}$ and $LP_{11}^{(p,b)}$. The wavelength of the input signal was set to the peak gain wavelength of 1537 nm, while the signal power was −10 dBm per mode. Since the pump laser produces a maximum output power of 26.5 dBm, the highest powers displayed in the horizontal axes of Fig. 3 for $LP_{21}^{(p,f)}$ and $LP_{11}^{(p,b)}$ pumping are 16.9 dBm and 19.3 dBm, respectively. The measured gains are shown as triangles for $LP_{01}^{(s)}$, and crosses for $LP_{11}^{(s)}$. The gain

#157732 - $15.00 USD Received 7 Nov 2011; revised 12 Dec 2011; accepted 13 Dec 2011; published 20 Jan 2012

characteristic shown in Fig. 3 matches the expectation that pumping in $LP_{01}^{(p)}$, in either forward or backward direction, leads to higher gain for $LP_{01}^{(s)}$, while pumping in higher order modes, significantly reduces this mode-dependent gain (MDG). In the case of forward $LP_{21}^{(p,f)}$ pumping scheme, modal gain for $LP_{01}^{(s)}$ and $LP_{11}^{(s)}$ are approximately equalized.

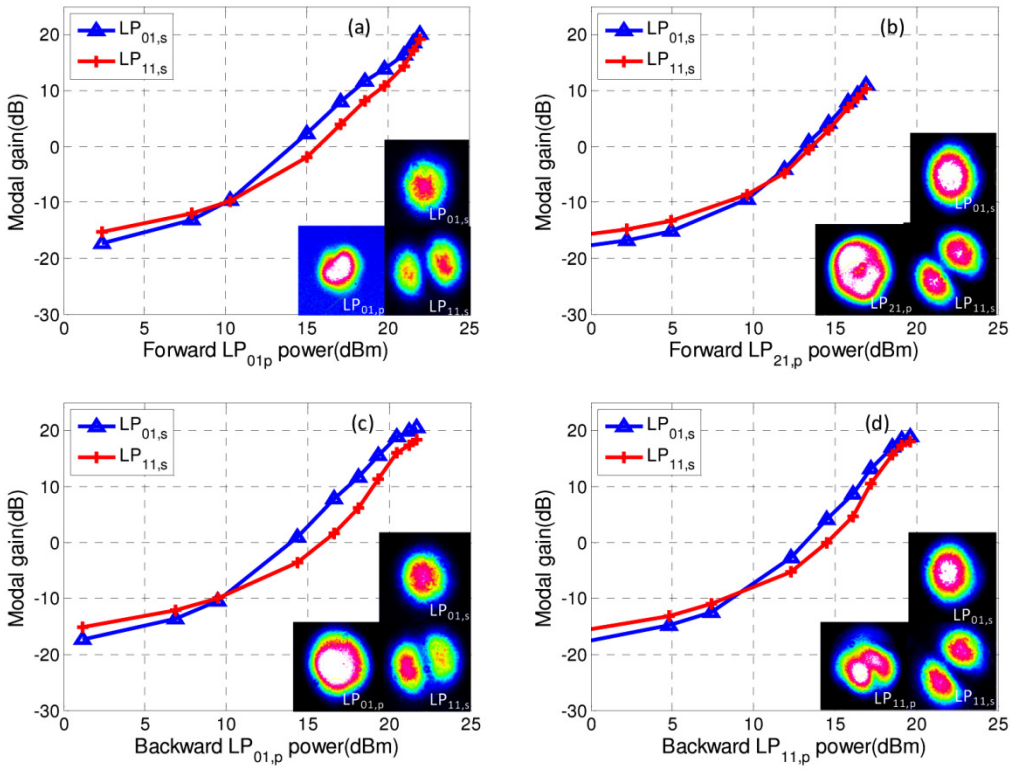

Fig. 3. Modal gain vs. Pump power when pumping forward in: (a) $LP_{01,p}$, (b) $LP_{21,p}$, and backward in(c) $LP_{01,p}$ (d) $LP_{11,p}$

Figure 4 (a) shows signal gain for $LP_{01}^{(s)}$ and $LP_{11}^{(s)}$ as a function of wavelength when pumped with 16.9 dBm of $LP_{21}^{(p,f)}$ or $LP_{11}^{(p,b)}$, at an input signal power of −10dBm. The shapes of the gain spectra match the typical emission spectrum of EDF. Figure 4 (b) shows MDG vs. wavelength. As a reference, MDGs for pumping in $LP_{01}^{(p)}$ for both forward and backward direction are also shown as blue lines. Although the $LP_{11}^{(s)}$ mode has less gain than $LP_{01}^{(s)}$ for both pumping method, we observe that pumping in $LP_{11}^{(p,b)}$ reduces MDG by ~1.3 dB at the peak gain wavelength of 1537 nm compared with pumping in $LP_{01}^{(p,b)}$. Moreover, pumping in $LP_{21}^{(p,f)}$ introduces even more MDG reduction which is 3.5dB. The total excursion of MDG across the C-band is also reduced from more than 3.5 dB to 2.5dB and 1 dB for $LP_{11}^{(p,b)}$ and $LP_{21}^{(p,f)}$ respectively.

#157732 - $15.00 USD Received 7 Nov 2011; revised 12 Dec 2011; accepted 13 Dec 2011; published 20 Jan 2012

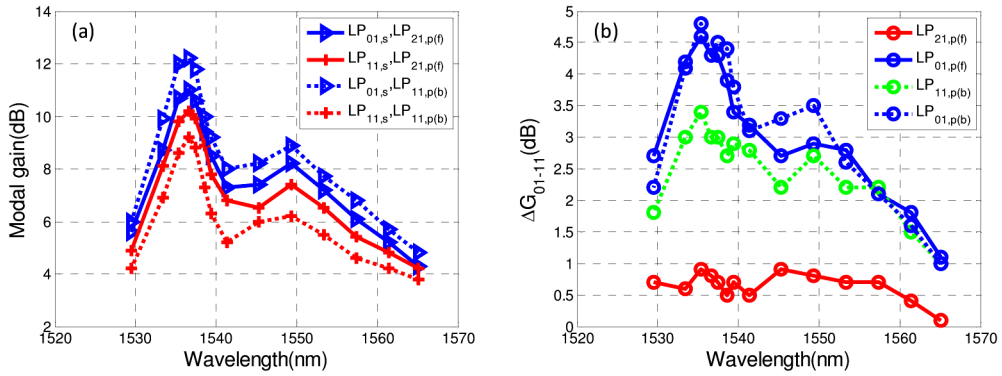

Fig. 4. (a) Modal gain vs. signal wavelength, using $LP_{21,p}$ (forward) and $LP_{11,p}$ (backward) and (b) MDG vs. signal wavelength using forward pumps in $LP_{01,p}$, $LP_{21,p}$ and backward pumps in $LP_{01,p}$, $LP_{11,p}$

3. Phase plates

In order to achieve high-efficiency crosstalk-free modal transformation, high optical quality phase plates with accurate optical transfer function are required. The fabrication process needs to provide an accurate, stable and steep phase transition between regions. For this purpose we designed, fabricated and characterized monolithic binary phase plates using a highly uniform Ag+/Na+ ion-exchange (IE) in glass, which provides important advantages compared to methods based on changing the thickness of the material. IE in glass is a well-established technique for material processing, integrated optics and other applications [9]. High precision and versatility are achieved through control of fabrication parameters such as diffusion time, temperature, diffusion coefficient, and the salt melt concentration. By using a Gaussian model together with the Inverse Wentzel-Kramer-Brillouin Method (IWKB) method, the desired phase-shift can be predicted by optimizing the refractive index variation of the Ion exchanged region. Phase plates designed for 1550 nm and 980 nm operation were fabricated with 5% $AgNO_3/NaNO_3$ salt melt at 340 °C. Multi-region binary plates were fabricated by using multi-region masks made by high-precision photolithographic techniques [10].

Phase plates were characterized by interferometry together with a modified Carré algorithm for the phase recovery. After phase is determined, an approximation technique for the diffusion time is used to improve the value of the required phase if necessary. The final phase value was set at 98% of the desired value (π radians) so tilting the phase plate by a small angle enables modal conversion be optimized.

4. Transmission experiment

The experimental setup is shown in Fig. 5. At the transmitter, 88 lasers (87 distributed-feedback (DFB) laser and one external cavity laser (ECL) for the channel measured) are divided into odd and even groups. Each group is separately modulated with 28 Gbaud QPSK, where the in-phase (I) and quadrature (Q) drive voltages are generated from pseudorandom binary sequence (PRBS) of length $2^{31}-1$. We generate polarization-multiplexed signals by splitting the modulator outputs, delaying one path by 405 symbols (14.46 ns), rotating it to the orthogonal polarization before polarization recombining. Odd and even channels are combined using an optical interleaver. The signal spectrum at the output of the single-mode transmitter is shown as an inset of Fig. 5. In the mode multiplexing circuit, the signal is split into three tributaries. Following decorrelation delays and amplification, the single-mode fibers are terminated at beam collimators (BC) with focal lengths of 11 mm. The beams propagating in free-space have $1/e$ radii of ~2 mm. For the LP_{11o} and LP_{11e} tributaries, phase plates with dual partitions having relative path delays of 0 and π radians at 1550 nm are used to spatially modulate the signal beam. Figure 6(a) shows the intensity patterns measured by a beam

#157732 - $15.00 USD Received 7 Nov 2011; revised 12 Dec 2011; accepted 13 Dec 2011; published 20 Jan 2012

profiler placed in the far field. We combine the three spatially orthogonal beams using passive beam splitters (BS), and the mode-division multiplexed (MDM) signal is launched into 50 km of FMF via an 11-mm BC. In this experiment, the relative difference in path lengths seen by the LP_{11o}, LP_{01}, and LP_{11e} tributaries (from the 1-by-3 splitter to the FMF input) are 0, 48.75 ns and 81.14 ns, respectively (corresponding to 0, 1365 and 2272 symbols). Thus, the minimum decorrelation delay between the six spatial-polarization modes is 405 symbols arising from the polarization multiplexer. This value is much greater than the modal group delay (MGD) of the FMF or the length of the time-domain equalizer used for MIMO demultiplexing, thus ensuring no spurious convergence where an equalizer output tributary obtains degenerate information from two different launched modes. The intensity patterns measured for the three spatial modes after 50-km transmission are shown in Fig. 6(b). Note that the LP_{11} patterns depend on the instantaneous coupling condition between odd and even modes, and is time-varying. We amplify the MDM signal using the FM-EDF considered in Section 2, with two 980 nm lasers pumps in forward and reverse directions. Pump and signal wavelengths are combined using free-space dichroic mirrors with insertion loss ~0.5 dB. Phase plates (designed for 980 nm) are used to spatially modulate the pumps. The forward-propagating pump is in the LP_{21} mode, while the backward-propagating pump is in the LP_{11} mode [6].

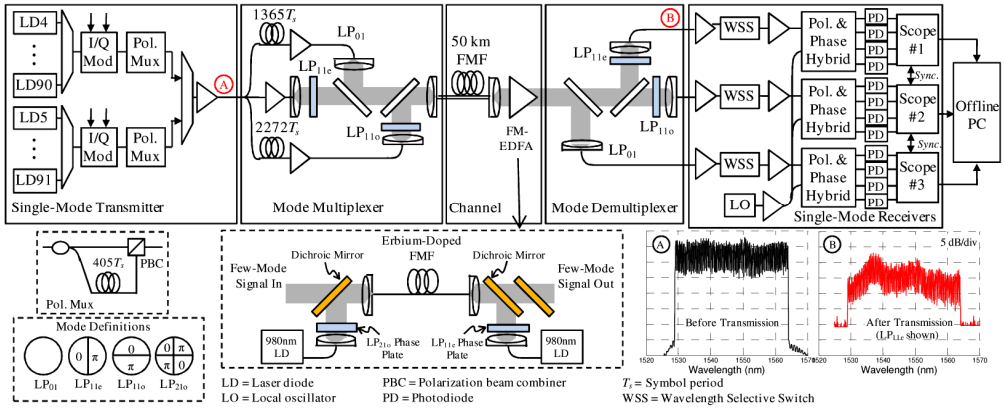

Fig. 5. Experimental setup.

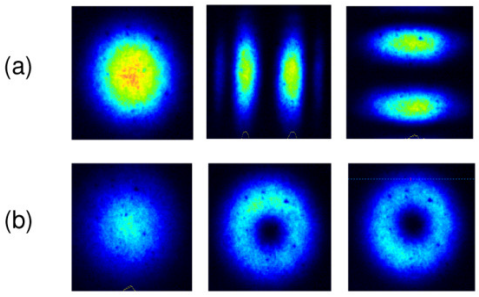

Fig. 6. (a) Intensity patterns at transmitter, (b) intensity patterns after 50-km FMF.

#157732 - $15.00 USD Received 7 Nov 2011; revised 12 Dec 2011; accepted 13 Dec 2011; published 20 Jan 2012

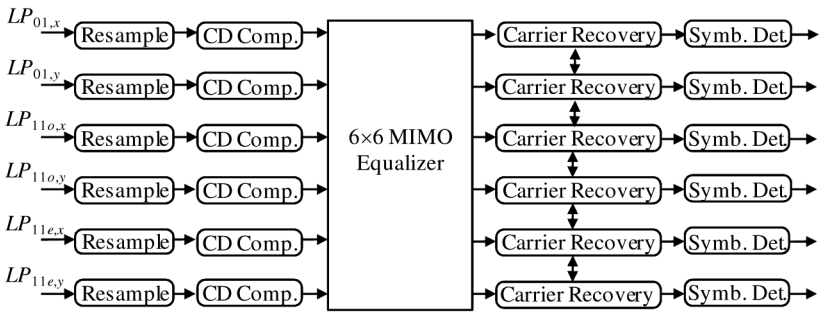

Fig. 7. Digital signal processing architecture.

At the receiver, the mode demultiplexer is a mirror image of the transmitter's mode multiplexer: we terminate the FMF at an 11-mm BC and use BSs to split the signal into three tributaries. In the LP_{11o} and LP_{11e} tributaries, the signal is spatially demodulated using phase plates. All three tributaries are then coupled back into single mode fibers using 11-mm BC. These signals are amplified and then filtered by wavelength selective switches (WSS). The channel of interest is downconverted to electrical baseband by mixing the signals with a common local oscillator (LO) laser using three polarization-and-phase diversity hybrids and twelve photodetectors, recovering the in-phase (I) and quadrature (Q) components of the six spatial-polarization modes. The electrical signals are sampled using three quad-channel sampling oscilloscopes with sampling rates and electrical bandwidths of 40 GSa/s and 16 GHz.

For data recovery, the digital signal processing algorithm shown in Fig. 7 is used. First, we upsample the signals to $M = 2$ times the baud rate (56 GHz). Optional frequency-domain equalizers (FDE) are used to compensate the average chromatic dispersion at (CD) of the LP_{01} and LP_{11} mode groups (see Section 6), followed by a 6×6 multiple-input multiple-output (MIMO) time-domain equalizer (TDE) that demultiplexes the six spatial-polarization modes. The operation of the equalizer can be generalized from [11]. Let $\mathbf{y}_k = \begin{bmatrix} \mathbf{y}_{1,k} & \cdots & \mathbf{y}_{N_m,k} \end{bmatrix}^{\mathrm{T}}$ be the vector of received samples used to recover symbol *k*, where $N_m = 6$ is the number of modes, and $\mathbf{y}_{i,k} = \begin{bmatrix} y_{i,Mk+L} & \cdots & y_{i,Mk-L} \end{bmatrix}^{\mathrm{T}}$ is a vector of $N = 2L+1$ complex-valued samples received at mode *i* at M times baud rate. The equations for MIMO equalization and equalizer update are given by:

$$\hat{x}_k = W^T y_k, \text{ and} \tag{1}$$

$$W \mapsto W + 2\mu y_k^* \varepsilon_k^T. \tag{2}$$

In Eq. (1), $\hat{\mathbf{x}}_k = \begin{bmatrix} \hat{x}_{1,k} & \cdots & \hat{x}_{N_m,k} \end{bmatrix}^{\mathrm{T}}$ is the equalized symbol, and $\mathbf{W}$ is the equalizer matrix

$$\mathbf{W} = \begin{bmatrix} \mathbf{W}_{11} & \cdots & \mathbf{W}_{1N_m} \\ \vdots & \ddots & \vdots \\ \mathbf{W}_{N_m1} & \cdots & \mathbf{W}_{N_mN_m} \end{bmatrix} \tag{3}$$

comprising $N_m \times N_m$ components $\mathbf{W}_{ij}$, each of which is a time-domain column vector of length N – i.e., $\mathbf{W}_{ij} = \begin{bmatrix} W_{ij,-L} & \cdots & W_{ij,L} \end{bmatrix}^T$. In the least-means square (LMS) update equation shown in Eq. (2), μ is the step size, and $\boldsymbol{\varepsilon}_k$ the error vector obtained for symbol *k*. In decision-aided (DA) mode, the transmitted symbol $\mathbf{x}_k$ is known, so $\boldsymbol{\varepsilon}_k = \mathbf{x}_k - \hat{\mathbf{x}}_k$; in decision-directed

#157732 - $15.00 USD Received 7 Nov 2011; revised 12 Dec 2011; accepted 13 Dec 2011; published 20 Jan 2012

(DD) mode, a symbol decision $\left[\mathbf{x}_k\right]_D$ is made on the equalized symbol $\mathbf{x}_k$, and the error $\boldsymbol{\varepsilon}_k = \left[\mathbf{x}_k\right]_D - \hat{\mathbf{x}}_k$ is the difference between the decision and its equalized value. For this experiment, we used a training sequence of 20,000 symbols for initial convergence of the TDE, at which point, the equalizer is switched to decision-directed (DD) adaptation. To ensure non-degeneracy of the outputs, we check the cross-correlation of the six output tributaries. In the experimental results presented in Sections 5 and 6, twenty data sets of 32,768 symbols were captured. For each data set, bit-error rate (BER) and Q-factor were computed from the second-half of the data after convergence of the TDE, (i.e., 655,360 bits per spatial-polarization modes were evaluated).

In this experiment, the coupling loss between single-mode fiber and the LP_{01} mode of the FMF is 1.8 dB, while the coupling loss between single-mode fiber and the LP_{11} of the FMF (the loss due to the phase plate is negligible) is 3.5 dB. The losses of the beam splitter are 2.8 dB (through) and 4.0 dB (reflected). The attenuation of the FMF are ~0.22 dB/km for the LP_{01} mode and ~0.25 dB/km for the LP_{11} mode. Summing these losses, the LP_{11o} and LP_{11e} modes have the highest total end-to-end loss of ~29.1 dB. The gains of the transmitter's single-mode fiber amplifiers were set so that all three spatial modes have the same power at the output of the FMF (i.e., before the FM-EDFA).

5. Experimental results

Figure 8 shows BER vs. OSNR curves for: (i) single-mode fiber back-to-back (BTB), (ii) MDM transmission BTB (via 1 meter of FMF), and (iii) after transmission for channel 38 at 1550.12 nm. It is observed that at a target BER of 10^{-3}, the OSNR penalty for cases (i) and (ii) with respect to the theoretical additive white Gaussian noise-limited BER vs. OSNR curve for QPSK are 1.2 dB and 2.8 dB, respectively. The similar penalties experienced by all three spatial modes in case (ii) indicate the channel matrix is approximately unitary. For case (iii), we used a TDE of 301 taps per tributary to compensate MGD and CD (i.e., no FDE was used). The length of the TDE was sufficient to overcome the MGD of the channel (see Section 6). The larger OSNR penalties for the higher-order LP_{11o} and LP_{11e} modes are caused by a combination of mode coupling at the MM-EDFA and mode-dependent gain in the amplifying medium causing the channel matrix to be non-unitary.

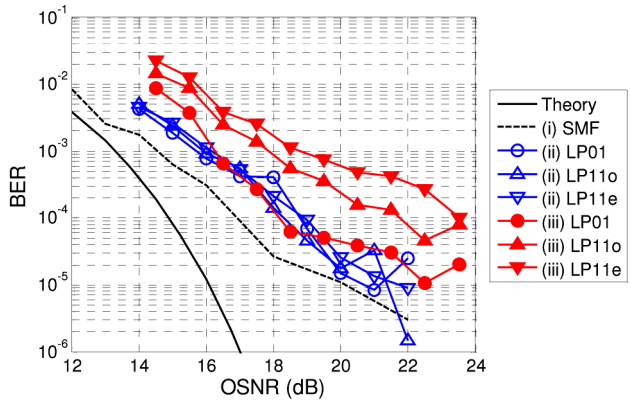

Fig. 8. BER vs. OSNR.

Figure 9 shows an example of the TDE obtained after convergence. The subplot at the intersection of the *i*-th row and *j*-th column is the vector $\mathbf{W}_{ij} = \left[W_{ij,-L} \quad \cdots \quad W_{ij,L}\right]^T$ as outlined in Section 4. In this experiment, we used $M = 2$ times oversampling and $N = 301$ taps for the TDE, which corresponds to a time span of 151 symbols sufficient to overcome the channel's MGD. The vertical axis in each subplot is the value (real and imaginary

#157732 - $15.00 USD Received 7 Nov 2011; revised 12 Dec 2011; accepted 13 Dec 2011; published 20 Jan 2012

components shown) of the filter coefficient, and the horizontal axis is the time index $-L \le l \le L$. We aligned the training symbols with the received signal in such manner that the coefficient at $l = 0$ is about halfway between the arrival times of the LP_{01} and LP_{11} modes. The coefficients $l > 0$ are the causal coefficients, and the coefficients $l < 0$ are anti-causal coefficients.

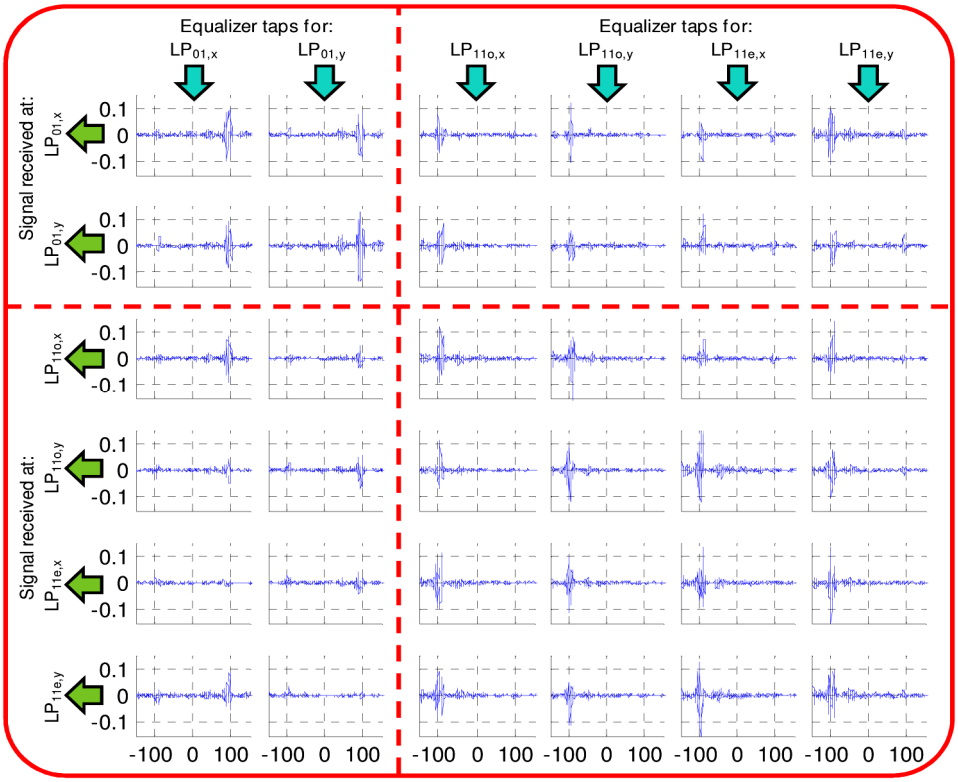

Fig. 9. Time-domain equalizer taps after convergence.

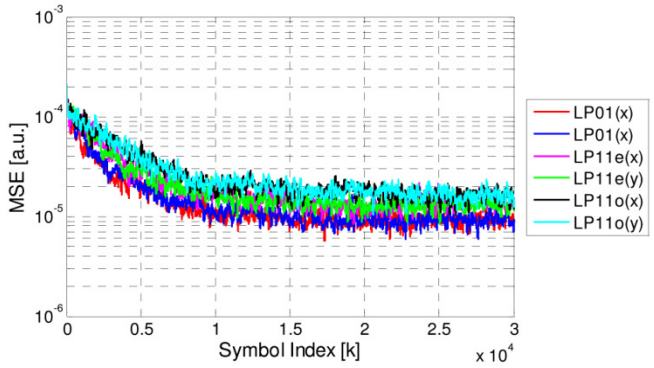

Fig. 10. Training characteristic: Mean square error vs. adaptation period.

From the equalizer description provided in Eq. (1) the columns of Fig. 9 (left to right) are the TDE coefficients used to recover the symbols transmitted in the $LP_{01,x}$, $LP_{01,y}$, $LP_{11o,x}$, $LP_{11o,y}$, $LP_{11e,x}$ and $LP_{11e,y}$ modes; while the rows denote the TDE coefficients operating on the outputs recovered at the $LP_{01,x}$, $LP_{01,y}$, $LP_{11o,x}$, $LP_{11o,y}$, $LP_{11e,x}$ and $LP_{11e,y}$ ports of the

#157732 - $15.00 USD Received 7 Nov 2011; revised 12 Dec 2011; accepted 13 Dec 2011; published 20 Jan 2012

coherent receiver. The principle sub-matrices of the TDE are the 2×2 sub-matrix at the top-left quadrant and the 4×4 sub-matrix at the bottom-right quadrant, which denote energy transmitted in one mode group being received at the ports of that mode group. Most of the energy in these submatrices is concentrated around a single peak corresponding to the expected arrival time for a signal propagating in that mode group in the FMF. The lack of spurious peaks indicates negligible multipath interference (MPI), where energy launched into one mode group is coupled to another mode group and then back again. By contrast, the off-diagonal sub-matrices denote energy transmitted in one mode group being received at the ports of the other mode group. This arises from mode mixing either at the transmitter, the FM-EDFA or the receiver. Considering the 4×2 sub-matrix in the bottom-left quadrant, the right-most peak denotes the signal propagating in the LP_{01} mode in the FMF, but is received at an LP_{11} port, while the left-most peak denotes the LP_{01} signal is coupled to LP_{11} at the transmitter, which propagates in the LP_{11} mode in the FMF and is received at an LP_{11} port. The temporal separation between the two peaks is the modal group delay in the 50-km FMF, which in this instance is around 91 symbols (3.25 ns), corresponding to a MGD of 65 ps/km. The dispersed peaks of the LP_{01} and LP_{11} modes arise from CD. Figure 10 shows a typical training characteristic, where it is observed the TDE taps converged after ~10,000 symbols.

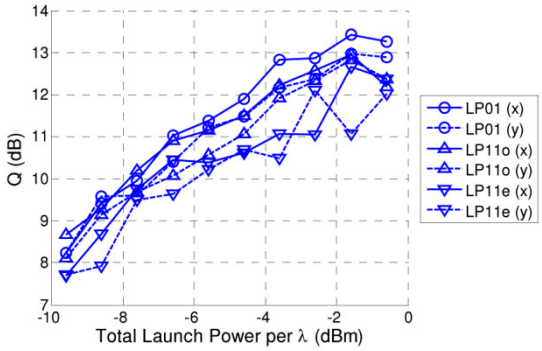

Fig. 11. Q vs. Launch Power after transmission.

Figure 11 shows Q vs. launch power after transmission. It is observed that the Q-factor is still increasing at the highest power, indicating that the system remains in the linear regime even when the transmitter's EDFAs are set to their maximum output powers. System performance is therefore limited by the combined amplified spontaneous emission (ASE) of the FM-EDFA and single-mode EDFAs. In Fig. 12, the BERs after transmission is shown for all the channels at the optimal launch power of –0.5 dBm/λ. It is observed that the BER of all modes of all the WDM channels are below the threshold of 3.8×10^{-3} for 7% hard-decision forward-error correction (HD-FEC) code. The BERs at the short wavelengths (right-hand side) are slightly higher due to the gain vs. wavelength characteristic of the MM-EDFA. The constellations of the best (Ch. 48) and worst (Ch. 88) channels are shown in the insets.

From the TDE taps observed in Fig. 9, it is possible to achieve significant reduction in algorithmic complexity by keeping only those equalizer taps with significant energy around each peak. Additionally, the number of significant taps at each peak can be reduced by compensating known CD using the FDE shown in Fig. 7. Figure 13 shows Q penalty vs. number of taps (N_{taps}) per TDE tributary, where half of the taps are allocated around each peak centered at the LP_{01} and LP_{11} arrival times. It is observed that to achieve Q penalty less than 1 dB, around 80 taps per tributary is required.

#157732 - $15.00 USD Received 7 Nov 2011; revised 12 Dec 2011; accepted 13 Dec 2011; published 20 Jan 2012

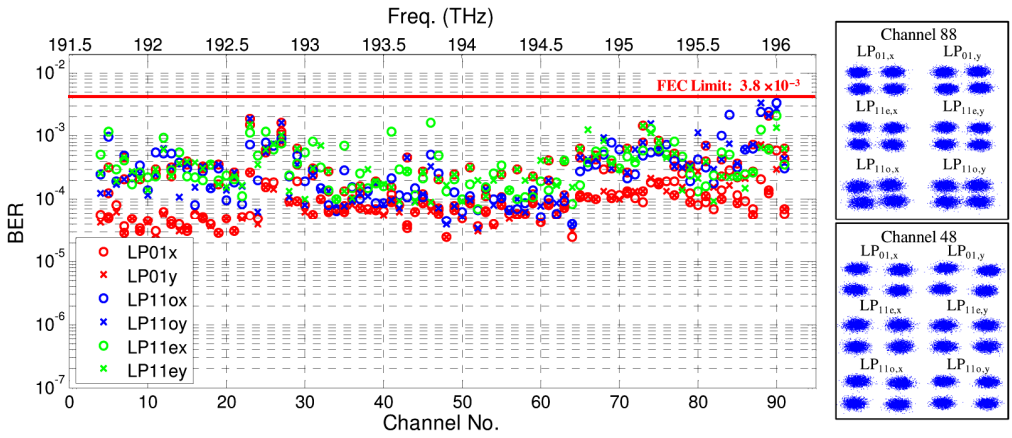

Fig. 12. Measured BER for all WDM channels after transmission. Insets: Constellation diagrams of best and worst modes.

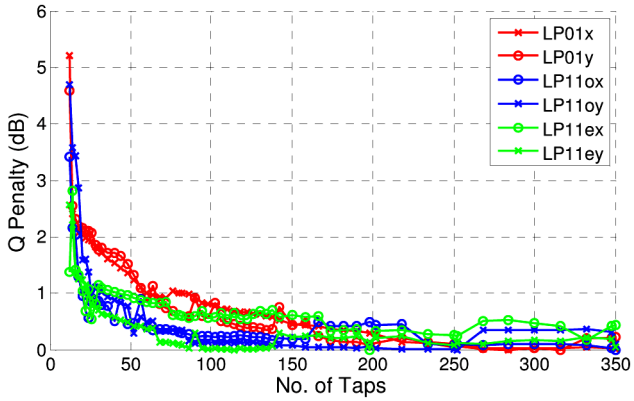

Fig. 13. Q penalty vs. No. of taps per tributary of 6 × 6 equalizer.

6. Fiber characterization

The FMF has a graded index core that was optimized to simultaneously achieve large effective area, low MGD and low coupling between the LP_{01} and LP_{11} modes. The calculated effective areas of the LP_{01} and LP_{11} modes are 137 and 183 μm^2, respectively, and the calculated MGD and chromatic dispersion are plotted in Fig. 14. The MGD of all the channels can be estimated experimentally from the equalizer coefficients after convergence. Figure 15(a) shows the results, where it is observed that MGD varies from 50 to 80 ps/km across the C-band. In addition, the use of training symbols enables measurement of the change in group delay with channel wavelength, and hence the CD of each mode of the FMF. The results are shown in Fig. 15(b). It is observed that the CD of the LP_{01} and LP_{11} modes at 1550 nm are around 20.5 and 19.8 ps/nm/km, respectively. The fluctuations of the data points from the regressive lines is due to measurement "noise" which arises from temperature drift as the channels are swept – i.e., small changes in either refractive index and fiber length will cause a change in the arrival time of the signal (group delay) independent of chromatic dispersion. To reduce measurement noise, we captured the channel sweep in ascending order of channel number as rapidly as possible to reduce thermal fluctuations. The measured differential MGD and chromatic dispersion agree well with the calculated values.

To characterize the fiber attenuation, we took OTDR traces with different offset launch positions with a standard single mode fiber. When there is no offset, it is expected that most light is launched into the LP_{01} mode. When the offset increases, more and more light will be

#157732 - $15.00 USD Received 7 Nov 2011; revised 12 Dec 2011; accepted 13 Dec 2011; published 20 Jan 2012

launched into the LP_{11} mode. Figure 16 shows OTDR traces for seven different launch positions. The attenuation increases slightly from 0.243 dB/km to 0.252 dB/km from center to 12 μm offset, indication very small attenuation difference between the LP_{01} and LP_{11} mode.

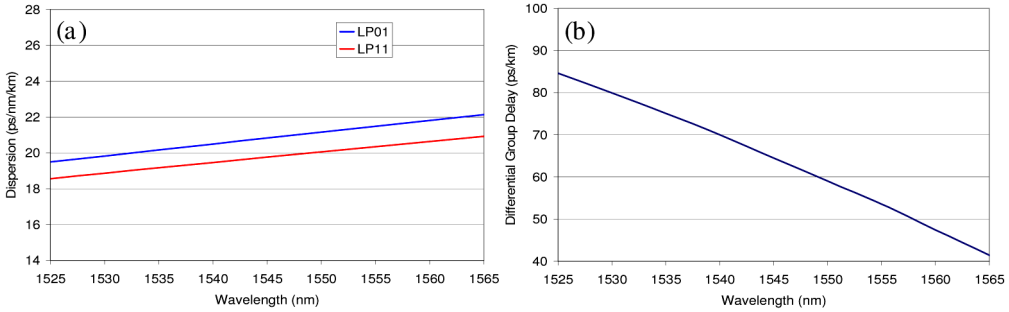

Fig. 14. Predicted (a) differential mode group delay and (b) chromatic dispersion.

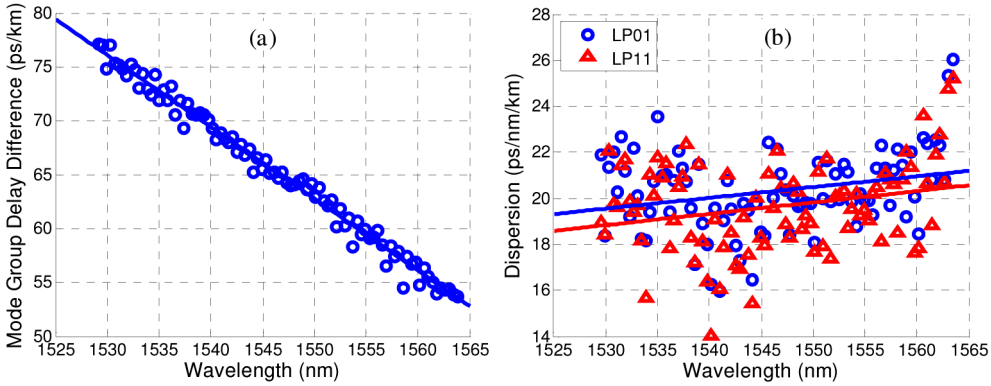

Fig. 15. Measured (a) differential MGD and (b) dispersion characteristic for experimental FMF.

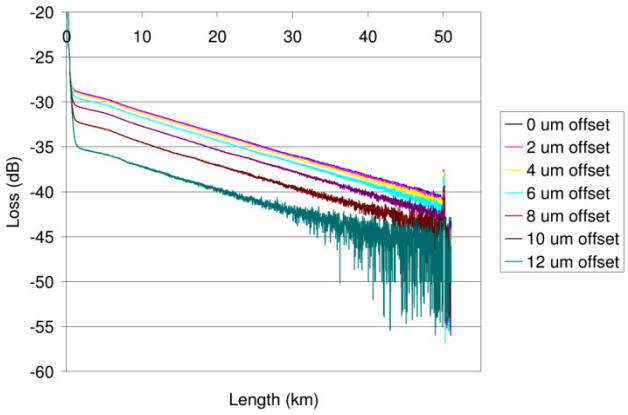

Fig. 16. Measured OTDR traces at different offset launch positions.

7. Conclusion

We successfully transmitted a 26.4 Tb/s mode-division multiplexed DWDM signal over 50-km of few-mode fiber with an inline few-mode EDFA before the receiver. Phase plates and free-space optics were used for spatial mode multiplexing and demultiplexing. The received signal was detected using three synchronized coherent receivers. We compensated mode coupling, modal group delay and chromatic dispersion using a digital 6 × 6 × 301 MIMO

#157732 - $15.00 USD Received 7 Nov 2011; revised 12 Dec 2011; accepted 13 Dec 2011; published 20 Jan 2012

equalizer. We also characterized the mode-dependent gain of the few-mode EDFA, as well as the differential modal group delay and dispersion characteristics of the transmission few-mode fiber.

Our experiment was ultimately limited by ASE noise of the receiver's single-mode EDFAs. We attribute this to the high loss of the receiver's spatial demultiplexer. To enable longer transmission distance, it is possible to (i) use a spatial hologram to demultiplex the MDM signal without the high losses incurred by the current spatial demultiplexer, and (ii) use a higher-gain FM-EDFA to boost the MDM signal power above sensitivity. In particular, it is necessary for the gain of the FM-EDFA to be at least equal to the span loss in both mode groups of the FMF in order to enable multi-span transmission using a recirculating loop.

#157732 - $15.00 USD Received 7 Nov 2011; revised 12 Dec 2011; accepted 13 Dec 2011; published 20 Jan 2012